Carbohydrate Polymers 298 (2022) 120148

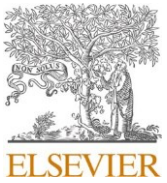

Contents lists available at ScienceDirect

Carbohydrate Polymers

journal homepage: www.elsevier.com/locate/carbpol

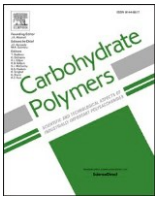

Application of yellow mustard mucilage and starch in nanoencapsulation of thymol and carvacrol by emulsion electrospray

Anto Pradeep Raja Charles [a], Richard Mu [b], Tony Z. Jin [c], Deyu Li [d], Zhiliang Pan [d], Sudipta Rakshit [a], Steve W. Cui [e], Ying Wu [a,*]

[a] Food Biopolymers Laboratory, Department of Agricultural and Environmental Sciences, Tennessee State University, Nashville, TN 37209, USA
[b] TSU Interdisciplinary Graduate Engineering Research Institute (Tiger Institute), Tennessee State University, Nashville, TN 37209, USA
[c] U.S. Department of Agriculture, Agricultural Research Service, Eastern Regional Research Center, Wyndmoor, PA 19038, USA
[d] School of Engineering, Vanderbilt University, Nashville, TN 37235, USA
[e] Guelph Research and Development Centre, Agriculture and Agri-Food Canada, ON N1G 5C9, Canada

ARTICLE INFO

Keywords:
Controlled release kinetics
Electrospray
Essential oil
Starch
Yellow mustard mucilage

ABSTRACT

Starch/water soluble yellow mustard mucilage nanocapsules loaded with thymol and carvacrol (TC) were developed using electrospray atomization. Emulsions were electrosprayed, aiming to generate nanocapsules with a controlled release behavior of TC for antimicrobial packaging applications. To understand the effect of water soluble yellow mustard mucilage (WSM) on the nanocapsules, the emulsion viscosity, morphology, encapsulation efficiency, molecular interactions, and release kinetics were evaluated. Surface and internal morphological analysis revealed that nanocapsules were non-porous with minimal surface shrinkages and had inner multicore spheres within a solid wall layer. Encapsulation efficiency ranged from 61.17 to 84.10 %, increasing at higher TC contents. Fourier transform spectroscopy confirmed the molecular interaction between wall materials. The release kinetics of encapsulated TC (30 % w/w) followed a Fickian diffusion mechanism and a controlled release pattern up to 120 h. Results indicated that the addition of WSM can modulate the release kinetics of bioactives and achieve a controlled release pattern.

1. Introduction

The fabrication and applications of natural polymers in food packaging are growing significantly due to increased health and environmental awareness. Natural polymer usages render potential advantages compared to synthetic polymers due to their enhanced barrier efficiency, biocompatibility, non-toxicity, and biodegradability (Cheng et al., 2019). Recently, the potential of plant polysaccharides and proteins is being continuously explored to design active packaging materials (Atta et al., 2022).

Antimicrobial food packaging is a novel approach of producing packaging materials containing active compounds (antimicrobials) to enhance the quality and safety of food. Based on the movement of active compounds from the packaging matrix, antimicrobial packaging is classified into migratory and non-migratory systems (Zhang, Jiang, Rhim, Cao, & Jiang, 2022). The migration of bioactives into the headspace of the packaging container acts as an excellent antimicrobial environment that could inhibit the growth of surface microorganisms and prolong food shelf-life (Kuai et al., 2021). Designing antimicrobial active systems that release bioactive compounds in a controlled manner could reduce food contamination, spoilage, and wastage (Limbo & Khaneghah, 2015).

Thymol and carvacrol ($C_{10}H_{14}O$) are important phenolic metabolites extracted from the thyme and oregano oils, respectively. Both carvacrol and thymol are highly volatile, generally recognized as safe (GRAS) additives, and exhibit synergistic antimicrobial effects (Marchese et al., 2016). However, their poor thermal and chemical stability and unpleasant taste make them unsuitable for active packaging (Shakeri, Razavi, & Shakeri, 2019). These limitations can be masked using the encapsulation process. Emerging advanced nano- and microencapsulation techniques can protect the bioactive compounds from degradation and mask undesirable flavors by enclosing them inside a stable polymer matrix (Niu, Shao, Luo, & Sun, 2020). The release kinetics, bioavailability, solubility, thermal stability, and mechanical property of

* Corresponding author at: Food Biopolymers Laboratory, Department of Agricultural and Environmental Sciences, Tennessee State University, 3500 John A Merritt Blvd., Nashville, TN 37209, USA.
E-mail address: ywu@tnstate.edu (Y. Wu).

https://doi.org/10.1016/j.carbpol.2022.120148
Received 1 July 2022; Received in revised form 7 September 2022; Accepted 20 September 2022
Available online 24 September 2022

bioactive substances can be improved by encapsulating them in suitable biopolymers (P´erez-Co´rdoba et al., 2018; Rehman et al., 2019).

Electrohydrodynamic processing is a drying technique that generates particles and fibers using electric field strength. Particles are produced by electrospray and fibers via electrospinning (Charles, Jin, Mu, & Wu, 2021). Electrospray is a non-thermal encapsulation process that employs an electric field to atomize the liquid droplets into micro or nanoparticles. Electrospray is suitable for entrapping sensitive bioactive compounds (core materials) inside a polymer matrix (wall materials). It preserves the biological and chemical functionalities of the encapsulated materials due to room temperature operation. For instance, a recent study indicated that the *Tinospora cordifolia* extracts possess antidiabetic activity (Jain et al., 2021). However, the poor release kinetics of extract and low bioavailability limit its nutraceutical application. Electrospray encapsulation of *Tinospora cordifolia* extracts in whey protein provided a controlled release pattern, improved bioavailability, and increased the anti-diabetic activity by 28.12 %. In another study, the thermal and photo-stability of D-limonene were improved by electrospray encapsulation using κ-carrageenan as wall material (Fani, Enayati, Rostamabadi, & Falsafi, 2022). Encapsulating the core material inside the polymeric matrix improves its bioavailability, stability, and controlled releasing ability (Ghorani & Tucker, 2015). The fabricated materials possess uniform morphology, smaller diameter, and large surface area per unit mass (Niu, Shao, Luo, & Sun, 2020). In addition, higher accessibility of atoms due to the expanded surface region gives rise to new physicochemical properties. The structure of the wall matrix performs an important role in modulating the releasing pattern of the core materials. For food packaging materials, natural polymers are considered an optimum option because of their environmental and safety advantages. Our recent study has summarized the significance of electrospray and electrospinning for developing active packaging materials using plant polysaccharides (Charles et al., 2021).

Water-soluble yellow mustard mucilage (*Sinapis alba* L.) is a natural polymer extracted from the yellow mustard bran using water (Wu, Eskin, Cui, & Pokharel, 2015). Water-soluble yellow mustard mucilage (WSM) is a novel ingredient that contains *heterogeneous* mixtures of acidic and neutral polysaccharides (Cui, Eskin, Wu, & Ding, 2006). The acidic and neutral fractions are in the proportions of 53 % and 47 %, respectively. The acidic fractions are pectic polysaccharides and fragments of β-1,4-linked glucose with additional oligosaccharide side chains. The WSM shows superior surface activity, antioxidant property, and emulsion stability (Wu et al., 2015; Wu, Hui, Eskin, & Cui, 2016). Mainly it exhibits interactions with starch resulting in increased viscosity and mechanical properties, namely hardness, springiness, adhesiveness, and chewiness (Liu, Eskin, & Cui, 2003). Thus far, no study has discovered the potential of WSM in encapsulating bioactive compounds.

The current study hypothesized that the synergistic interactions between WSM and potato starch could be used to fabricate capsules for encapsulating different concentrations of thymol and carvacrol mixture (TC) by electrospray. The resultant materials could be used for antimicrobial active packaging as the polymer matrix could modulate the release pattern of TC. The study has optimized the emulsion formulation and viscosity to fabricate uniform non-porous nanocapsules through electrospray. The generated capsules were evaluated in terms of surface and internal morphological properties, encapsulation efficiency, molecular interaction, and release kinetics of TC using mathematical drug release models.

2. Materials and methods

2.1. Materials

Yellow mustard bran was procured from Wisconsin Spice, Inc. (Berlin, WI, USA). Soluble potato starch (Mw 342.29 g/mol), thymol, carvacrol, and Tween 20 were purchased from Fisher Scientific (Waltham, MA, USA). Absolute ethanol (>99.9 %), formic acid, and dialysis tube were obtained from Sigma-Aldrich (St. Louis, MO, USA). Phosphate-buffered saline (PBS) and ethyl acetate were purchased from VWR International (West Chester, PA, USA). The deionized water (18.2 MΩ·cm) was prepared using the Milli-Q® purifier (Sigma-Aldrich, St. Louis, MO, USA).

2.2. Extraction of WSM

The extraction of WSM was performed using the method explained by Wu et al. (2016). Briefly, the yellow mustard bran was steeped for 2 h in deionized water (70 °C) at the solid to liquid ratio of 1:12 (w/v) with continuous stirring. The solution was filtered using a cheesecloth followed by centrifugation at 1184 rad/s (11,306 rpm) for 15 min to separate the water-insoluble fraction. The supernatant was treated using ethanol (100 %) to precipitate the soluble mucilage. Further, the residue was dried in the fume hood and stored at 4 °C for further analysis. The proximate analysis performed in triplicates revealed that the WSM contains carbohydrates (88 %) as major portions, and the minor constituents were protein (4.4 %) and ash (3.1 %). The molecular weight of WSM was 4380 kDa.

The WSM residues were dissolved at 65 °C deionized water with constant stirring for 1 h to prepare WSM solution (2 % w/v).

2.3. Preparation of starch solution and oil-in-water emulsions

Starch solution (30 % w/v) was prepared using formic acid (75 %). The solution was stirred at 50 °C for 9 h for retrogradation and later stored overnight at 3 °C to regain its crystalline structure.

The above-prepared starch and WSM solution were mixed at the ratio of 3:1 (v/v) to form a Starch-WSM (SW) base solution. Thymol and carvacrol were added to the SW solution at a ratio of 1:1 (w/w) to achieve the final TC concentrations (10, 20, or 30 % w/w), thereby forming $SWTC_{10}$, $SWTC_{20}$, and $SWTC_{30}$ formulations. Emulsions prepared without WSM but starch and TC were also electrosprayed at the TC concentration of 30 % (w/w) (STC_{30}) to study the modulating effect of WSM on releasing kinetics of TC. The pre-homogenization of emulsions (50 mL) was carried out at 11,000 rpm for 1 min using a polytron (PT 3000, Kinematica Inc., Lucerne, Switzerland), followed by three passes into a microfluidizer (LM20 Microfluidizer, Microfluidics Inc., MA, USA) at 103.4 MPa.

2.4. Shear rheology measurements

Rheological characteristics of the emulsions were analyzed using a Rheometer (Ares G2 Rheometer, TA Instruments, DE, USA). The apparent viscosity was measured with the shear rate ramps from 0.01 to 100 s^{-1} using a parallel plate geometry (40 mm diameter). All samples were measured in triplicates at 23.0 ± 0.5 °C.

2.5. Encapsulation through emulsion electrospray

Electrospray apparatus was designed with multiple needle spinneret to increase production efficiency. Emulsions were loaded to a 15 mL plastic syringe and directed towards the tip of the stainless-steel needle (outer diameter 0.91 mm, inner diameter 0.6 mm) using an infusion pump at the fixed rate of 0.10 mL·h^{-1}. Direct current supply of 22 kV performed atomization, and the capsules were collected in an aluminum foil positioned 12 cm away from the needle tip. All the samples were electrosprayed at the ambient temperature (23.0 ± 0.5 °C). The schematic representation of capsule generation by electrospray is shown in Fig. 1.

2.6. Characterization of particles properties

2.6.1. Process yield

The amount of nanocapsules obtained through electrospraying was

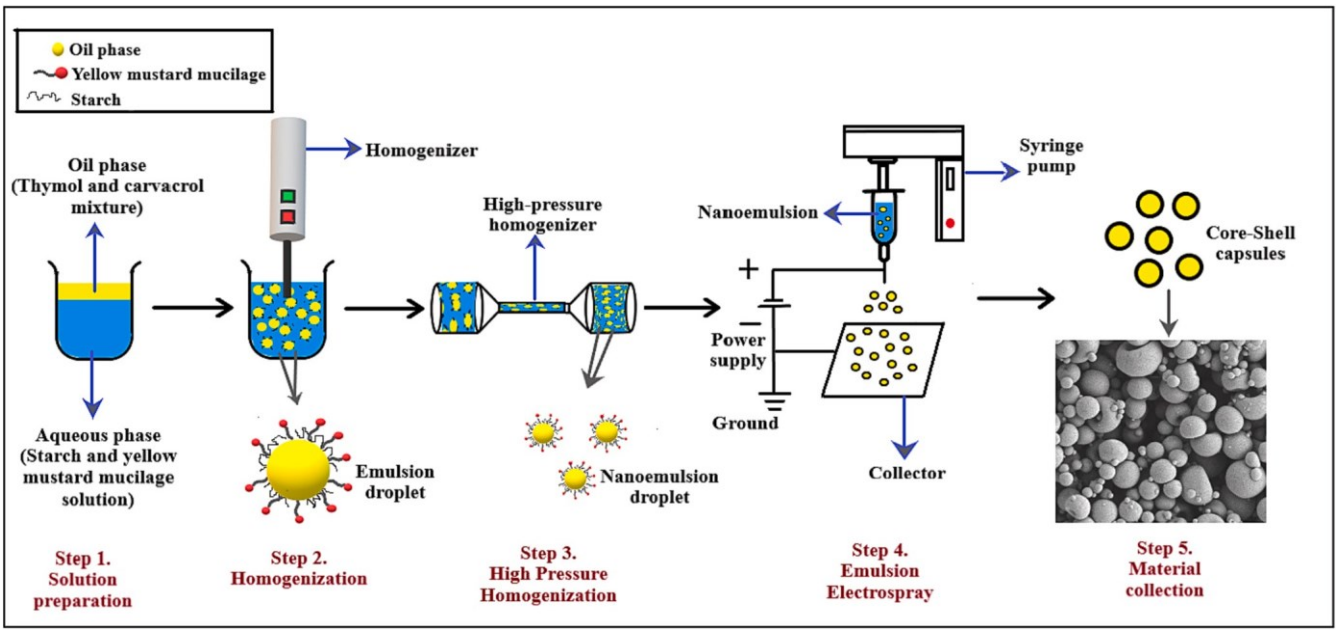

Fig. 1. Schematic illustration of electrospraying process for capsule generation.

calculated gravimetrically with respect to the percentage of solid contents added during the emulsion preparation.

2.6.2. Encapsulation efficiency

The total and surface TC content of the capsules were measured to calculate the encapsulation efficiency. For determining the total TC content, 10 mg of capsules were suspended in ethyl acetate (2 mL) for 24 h to release the TC completely. Then the solution was centrifuged at 10,000 rpm for 10 min and filtered using PTFE membranes (0.2 mm Whatman Filter, GE Healthcare, Piscataway, NJ, USA). The obtained supernatant was measured spectrophotometrically (UV–Vis spectrophotometer, Agilent Technologies, Wilmington, DE, USA) at 274 nm (maximum absorbance for thymol and carvacrol (Hajimehdipoor, Shekarchi, Khanavi, Adib, & Amri, 2010)) and analyzed using a calibration curve ($R^2 = 0.993$) generated using thymol-carvacrol (1:1) in ethyl acetate.

Similarly, the surface TC content was determined by suspending 10 mg of capsules in 2 mL of ethyl acetate and vortexed for 40 s. The centrifugation was performed at 1000 rpm for 1 min, and the supernatant was analyzed. Spectrophotometric measurements were not interfered by starch and WSM due to their insolubility in ethyl acetate.

The total TC, surface TC, and encapsulation efficiency of the capsules were calculated using the following equations (Niu, Shao, & Sun, 2020).

$$\textit{Total TC content}\ (\%) = \frac{\textit{total TC content in capsules}}{\textit{theoretical amount of TC added to emulsions}} \quad (1)$$

$$\textit{Surface TC content}\ (\%) = \frac{\textit{surface TC content in capsules}}{\textit{theoretical amount of TC added to emulsions}} \quad (2)$$

$$\textit{Encapsulation efficiency}\ (\%) = \frac{\textit{total TC} - \textit{surface TC}}{\textit{total TC}} \times 100 \quad (3)$$

2.6.3. Surface morphology using a scanning electron microscope (SEM)

The morphology of electrospray capsules was analyzed using a scanning electron microscope (Zeiss Merlin, Carl Zeiss Microscopy, Thornwood, NY, USA). Before analysis, sputter coating was performed under vacuum using the gold-palladium mixture. A working distance of 7 to 9 mm, magnification of 25,000×, and 10 kV accelerating voltage were fixed to capture images. The SEM micrographs were used to determine the size distribution of the capsules using ImageJ software (NIH, Bethesda, MD, USA). The diameter distribution was expressed in terms of the number of capsules, and the reported diameter was an average of 100 measurements. The polydispersity index (PDI) was calculated using the following equation (Paximada, Echegoyen, Koutinas, Mandala, & Lagaron, 2017).

$$PDI = \frac{D_{90} - D_{10}}{D_{50}} \quad (4)$$

where D_{10}, D_{50}, and D_{90} represent the capsule diameters at 10 %, 50 %, and 90 % cumulative volume, respectively.

2.6.4. Internal structure of capsules

Cross-sectional analysis was carried out using a focused ion beam technology equipped with a scanning electron microscope (FIB-SEM, Nanolab G3 CX, FEI Company, Hillsboro, OR, USA). During the analysis, the sample stage was titled 52° to make it perpendicular to the ion beam, promoting straight ion milling. Capsules were cut opened using the Ga^+ ion beam (16 kV, 11 pA), and SEM images were captured by the electron beam (5 kV, 86 pA) between ion beam cuts.

2.6.5. Molecular interaction

Fourier Transform Infrared (FTIR) spectroscopic analysis was performed to determine molecular interactions between TC and polymeric matrix. The spectra of fabricated capsules and individual compounds were acquired using an FT-IR spectrophotometer (PerkinElmer Frontier, PerkinElmer, Waltham, MA, USA). Samples were analyzed at room temperature (23.0 ± 0.5 °C) over the frequency range between 4000 and 500 cm^{-1} at 4 cm^{-1} resolution.

2.6.6. Release kinetics

The releasing profile of TC was performed using the dialysis tubing method. A dispersion containing 10 mg of encapsulated capsules was suspended into a dialysis tube (molecular weight cut-off range: 3500 Da) containing 20 mL of PBS (pH = 7.4) to adopt sink conditions. Further, the dialysis tubes were transferred into a beaker containing 100 mL of PBS, stirred gently (80 rpm), and maintained at 37 °C. A volume of 2 mL of aliquots of the sample at different time intervals (0–120 h) was removed, and the same amount of buffer was replaced. The TC release percentage was examined using a UV–Vis spectrophotometer (Agilent

Technologies, Wilmington, DE, USA) at the wavelength of 274 nm and quantified by a calibration curve generated using the release media ($R^2_{PBS} = 0.994$). The accumulative TC release percentage was calculated using Eq. 5.

$$TC\ release\% = (M_t/M_o) \times 100 \quad (5)$$

where M_t is the amount of TC (mg) released from the capsules at time t, and M_0 is the initial amount of TC (mg) in the capsules.

2.7. Statistical analysis

Experimentations were performed at least in triplicates using fresh samples, and the data were presented as mean value ± standard deviation. Statistical analysis was implemented using OriginPro 10.5 (OriginLab Corp., Northampton, MA, USA). One-way ANOVA and F-protected LSD were applied to evaluate the significance of difference among samples at a level $p < 0.05$.

3. Results and discussion

3.1. Rheological property

Emulsion viscosity is important as it influences particle morphology and encapsulation efficiency (Charles et al., 2021). In the rheogram (Fig. 2), emulsions displayed a shear thickening behavior between the shear rate of 0.01–0.06 s^{-1} and pseudoplastic or shear-thinning behavior at the intermediate shear rates (above 0.07 s^{-1}). Starch commonly exhibits shear thickening behavior at a low shear rate due to structure formation by amylopectin molecules, which open up and stretch to form intermolecular double helices that hold polymers together (Hamaker, 2021). In the mixed solutions containing starch and WSM, the large molecules will interact by physical entanglements and chemical associations via hydrogen bonding, thus causing resistance to flow, leading to shear thickening behavior at the lower shear range (Liu, Eskin, & Cui, 2006). However, at the intermediate shear rate, the molecular interactions are not strong enough to resist the flow, and the molecular network was disrupted, thus exhibiting the shear-thinning property.

Adding TC to the polymeric solution increased the viscosity at lower shear rates (0.01–0.06 s^{-1}) due to the increase in the packing fraction of hydrophobic droplets. It was reported that WSM contained a small amount (16 %) of cellulosic polysaccharides with methyl groups substituted at the 2, 3, 6 positions of the glucose residues (Wu, Cui, Eskin, Goff, & Nikiforuk, 2011). These hydrophobic groups may contribute to the hydrophobic bonding between polysaccharides and TC, thus leading to increased viscosity. Similar findings were observed in the emulsions prepared using menhaden oil, in which the low shear viscosity of emulsions increased with oil concentrations (Sun & Gunasekaran, 2009). However, as the shear rate raised above 0.07 s^{-1}, the increase in TC concentrations decreased the viscosity, attributed to the hydrophobic structures that prevent the intermolecular interactions between polymers and the inability of emulsions to resist the flow. Altan, Aytac, and Uyar (2018) indicated similar flow patterns in which the viscosity of zein emulsions decreased with increased carvacrol concentration at high shear rates.

During the emulsion preparation, the high-pressure microfluidization might cause a conformational change in the polymeric chain and deform the oil droplet leading to shear thinning behavior (McClements, 2015). During the electrospray process, the physical entanglements may be interrupted. Thus, the absence of enough chain entanglements in emulsions favored particle generation instead of fibers as jet fragmentation occurred due to weak intermolecular cohesive forces.

3.2. Electrospray yield and encapsulation efficiency

The electrospray parameters were optimized to form a Taylor cone. The process yield was >60 % for all capsules (Table 1). The variation in the process yield is attributed to the surface tension and conductivity

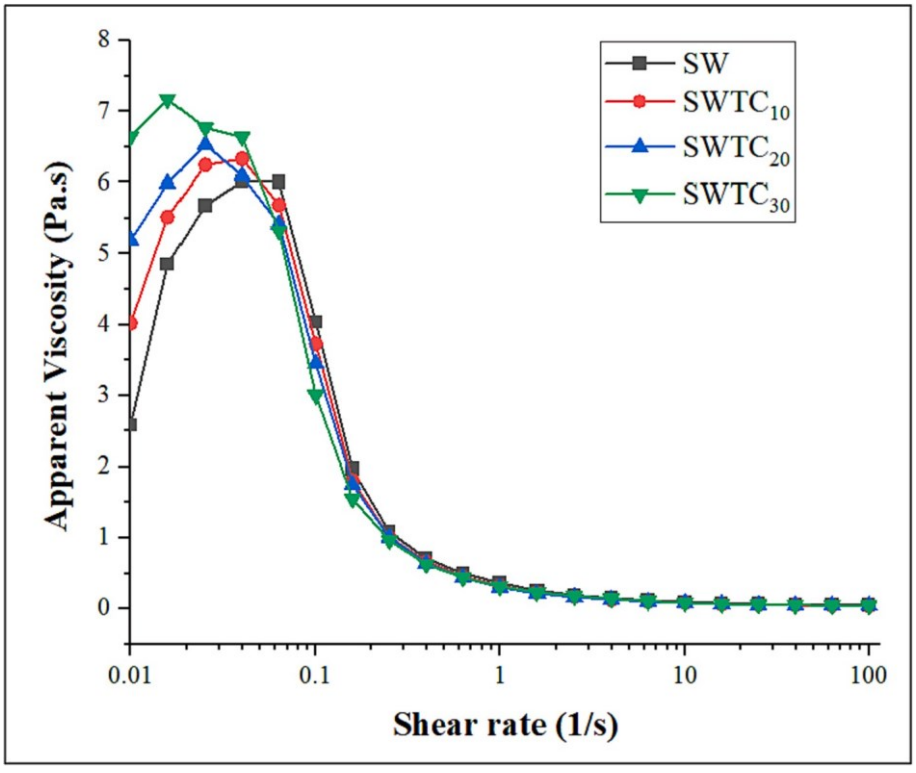

Fig. 2. Apparent viscosity of SW solution and $SWTC_{10}$, $SWTC_{20}$, and $SWTC_{30}$ emulsions at different shear rates. Abbreviations: SW, starch-water soluble yellow mustard mucilage; TC, thymol-carvacrol mixture; $SWTC_{10}$, SW with 10 % TC; $SWTC_{20}$, SW with 20 % TC; $SWTC_{30}$, SW with 30 % TC.

Table 1
Process yield, polydispersity index, total and surface TC contents, and encapsulation efficiency (EE) of the nanocapsules.

Nanocapsules	Process yield (%)	PDI	Total TC (%)	Surface TC (%)	Encapsulation efficiency (%)
$SWTC_{10}$	77.32 ± 1.7[b]	0.529[a]	70.11 ± 1.56[c]	27.24 ± 3.28[b]	61.17 ± 4.20[c]
$SWTC_{20}$	73.35 ± 0.6[c]	0.417[c]	80.92 ± 1.54[b]	17.72 ± 1.34[c]	78.11 ± 1.24[b]
$SWTC_{30}$	70.08 ± 1.2[d]	0.417[c]	84.91 ± 2.36[a]	13.49 ± 1.28[d]	84.10 ± 1.46[a]
STC_{30}	65.23 ± 0.9[e]	0.430[b]	61.34 ± 3.19[d]	33.41 ± 2.71[a]	45.53 ± 3.36[d]
SW	80.64 ± 1.4[a]	0.342[d]	–	–	–

differences between the feed solution, as they impact the stability of the Taylor cone (de Souza, Kringel, Dias, & da Rosa Zavareze, 2021).

Delivery carriers with high encapsulation efficiency (EE) are essential for commercial food and active packaging applications. The EE depends on the polymer properties, bioactive compounds' affinity towards the wall material, emulsion stability, solvent evaporation rate, and electrospray processing parameters (feed rate, needle diameter, distance between needle tip to collector, and electric field) (Charles et al., 2021).

Total TC content, surface TC content, and encapsulation efficiencies of capsules were estimated using UV–Vis measurements, and the findings are shown in Table 1. The mean EE of the electrospray capsules was between 61.17 *and* 84.10 %, varying based on TC concentrations. It was observed that the EE increased with the increase in TC concentration in the emulsions. Among Starch-WSM-TC (SWTC) emulsions, SWTC with 30 % TC ($SWTC_{30}$) capsules had the highest EE and the lowest surface oil content. This observation is attributed to their bigger particle size and thus smaller surface area, leading to more TC entrapment within the matrix. Besides, the higher emulsion viscosity may also help to retain the oils in the particles. In general, emulsions with higher viscosity are more stable during electrospray, thereby achieving superior entrapment efficiency (Atay et al., 2018). Also, high viscosity promoted faster solidification of the starch-WSM matrix, assisting in retaining volatiles. Other researchers have also observed considerable EE (81–88 %) during essential oil entrapment through electrospray (Rezaeinia, Ghorani, Emadzadeh, & Tucker, 2019). For example, a study on pectin-sodium alginate matrix to encapsulate carvacrol through spray drying has observed that the EE fell in the range of 45.73–82.79 % (Sun, Cameron, & Bai, 2020). Our results showed a better EE as the electrospray process occurs at room temperature, thus preventing the degradation and volatilization of thymol and carvacrol. For this reason, electrospray is exceedingly suitable for encapsulating heat-labile and volatile compounds.

P´erez-Masia´ et al. (2015) used starch matrix for encapsulating folic acid and observed a similar EE range. Starch is an excellent film-forming agent. Therefore, during electrospray, it could have prevented the thymol and carvacrol migration *towards* the surface of the capsules. In the current study, the starch matrix was used as a control. The result indicated that starch alone was insufficient to firmly encapsulate TC, leading to the generation of irregular structures (indicated in Fig. 3e). This irregularity may be due to the lack of structures among starch molecules; thus, the collapse occurred during the evaporation of TC and solvent molecules.

Different alphabets in the superscript of each value in the same column denote significant differences ($p < 0.05$). Abbreviations: PDI, polydispersity index, SW, starch-water soluble yellow mustard mucilage; TC, thymol-carvacrol mixture; $SWTC_{10}$, SW with 10 % TC; $SWTC_{20}$, SW with 20 % TC; $SWTC_{30}$, SW with 30 % TC; STC_{30}, starch with 30 % TC.

Upon the addition of WSM in the emulsion formula, it is evident that the encapsulation efficiencies are significantly increased ($p < 0.05$). This outcome could be ascribed to the synergistic interaction between the WSM and starch. The starch and WSM formed hydrogen bonding among molecules, thereby generating a hydrated layer at the droplets' surface (Liu et al., 2006). The presence of ethyl and methyl groups in WSM (Wu et al., 2011) could have retained the thymol and carvacrol during the electrospray process, leading to higher encapsulation efficiencies. In addition, WSM helped to generate a more stable emulsion and prevented the partitioning of core compounds (Wu et al., 2015).

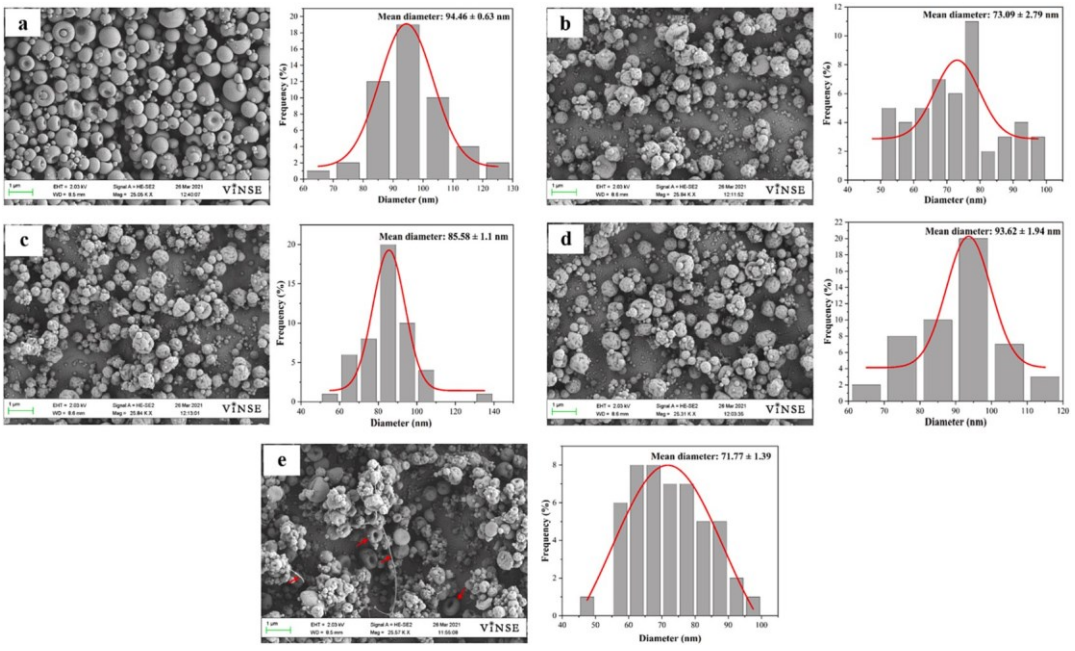

Fig. 3. SEM images and diameter distribution of electrospray nanocapsules: (a) SW (b) $SWTC_{10}$, (c) $SWTC_{20}$ (d) $SWTC_{30}$, (e) STC_{30}. Abbreviations: SW, starch-water soluble yellow mustard mucilage; TC, thymol-carvacrol mixture; $SWTC_{10}$, SW with 10 % TC; $SWTC_{20}$, SW with 20 % TC; $SWTC_{30}$, SW with 30 % TC; STC_{30}, starch capsules with 30 % TC.

3.3. Surface morphological properties of electrospray capsules

The fabricated capsules were analyzed using SEM to characterize their morphology and diameter distribution. The SEM images of Starch-WSM (SW), $SWTC_{10}$, $SWTC_{20}$, and $SWTC_{30}$ capsules and the diameter distribution are presented in Fig. 3. It is evident that the morphology of SW capsules (wall matrix) is spherical and possesses a continuous smooth surface (Fig. 3a). No surface cracks or pores were noticed in the capsules, thereby reducing gas permeability and enhancing the retention and protection of thymol and carvacrol. Thus, the fabricated wall matrix is suitable for encapsulating TC. The diameter of SW capsules was closely distributed in the range of 64 to 125 nm with a mean diameter of 94.46 ± 0.63 nm. Upon TC encapsulation, the $SWTC_{10}$, $SWTC_{20}$, and $SWTC_{30}$ carriers retained their spherical structures. The particle diameter gradually increased based on the TC concentrations. The mean diameter of $SWTC_{10}$ capsules was 73.09 ± 2.79 nm, which increased to 93.62 ± 1.94 nm for $SWTC_{30}$. Similar findings were observed by Li et al. (2013) in encapsulating thymol in the zein-sodium caseinate matrix and by Yilmaz et al. (2019) in encapsulation of *Origanum vulgare* oil in chitosan nanoparticles.

Compared to SW capsules, the encapsulated carriers had surface shrinkages. The thymol and carvacrol could have caused these shrinkages due to their impact on solvent evaporation. In addition, shrinkages and dents are commonly found across polymeric structures generated through the drying process due to the rapid evaporation of solvents (Cui, Kimmel, Zhou, Rao, & Chen, 2020).

As a comparison, the capsules were generated using only starch as the matrix with TC (30 % w/w). Irregular structures with a mean diameter of 71.77 ± 1.39 nm were observed, as shown in Fig. 3e. Moreover, intense agglomerations were noticed, which could be due to the increased amount of thymol and carvacrol on the capsules' surface. Therefore, the presence of WSM is vital in the emulsion formula for non-porous core-wall structure generation.

In addition to the surface morphology and capsule diameter, PDI is another critical characteristic of nanocapsules that indicates particle size dispersity. The PDI > 0.7 represents polydisperse, 0.1–0.7 represents moderately polydisperse, and 0.0–0.1 indicates monodisperse distribution (Human, De Beer, Van Der Rijst, Aucamp, & Joubert, 2019). In the current study, the SW capsules had the least PDI of 0.342 (Table 1), which increased upon adding TC. The PDI of encapsulated nanocarriers ranged from 0.417 to 0.529, indicating the capsules are moderately polydisperse. The presence of TC in the feed solution causes a change in conductivity that could reduce the area of the cone-jet region, thus causing moderate polydisperse distribution (Soleimanifar, Jafari, & Assadpour, 2020). A similar range of PDI was observed in electrosprayed zein/shellac particles encapsulated with thymol (Liu et al., 2021).

3.4. Internal structure of the capsules

$SWTC_{30}$ capsules were selected to analyze the internal structure and release kinetics due to their higher EE. FIB-SEM was used to examine the internal structure of $SWTC_{30}$ capsules by etching out their surface using Ga^{2+} ions. The cross-sectional images (Fig. 4) displayed the structure of capsules. Multiple-core spheres were noticed on the core space representing successful encapsulation of TC within the wall matrices. The capsules were mainly spherical due to the self-assembly of wall matrices as the solvent evaporates, which was confirmed through SEM and FIB-SEM images. Cross-section images revealed a single solid wall layer representing chain associations between WSM and starch molecules. They also are ascribed to the miscibility of WSM and starch. Primarily, capsules had a compact internal structure (Fig. 4b), which helps decrease the surface area to volume ratio and control the diffusivity of TC through the wall matrices that assist in sustained release behavior. During the study, presence of vacuoles or hollow pores in a few capsules was observed (Fig. 4c). It could be due to the trapped air during atomization or homogenization processes. Further, the solvent distribution may also influence the capsule structure. Initially, the droplet shrinks with solvent evaporation from the surface of the capsules, and the solutes tend to diffuse towards the core until a solid wall is formed. If the solvent droplet is trapped in the matrix and eventually evaporated, it could leave pores in the internal structures (Park & Lee, 2009).

3.5. Molecular interaction in electrospray capsules

The FTIR analysis was carried out to identify the molecular interactions between the WSM, starch, thymol, and carvacrol in the capsules. The spectra are displayed in Fig. 5. The spectrum of potato starch revealed a characteristic band between 3000 and 3600 cm^{-1} corresponding to stretching vibration of free intra- and inter-molecular bound hydroxyl groups. The stretching of C−H formed a small band visible at 2929 cm^{-1} (Hong, Chen, Zeng, & Han, 2016). The peak at 1641 cm^{-1} is ascribed to the bending vibration of H_2O molecules. The CH_2 deformation or C−O−H bending led to a specific band at 1351 cm^{-1}. The peaks observed on 1150 and 1080 cm^{-1} are due to the coupling reaction between C−O, C−C, and O−H bond bending and stretching. Also, it is ascribed to asymmetric stretching of C−O−C glycosidic bond (Capron, Robert, Colonna, Brogly, & Planchot, 2007). Further, the IR bands at 996 (C−O−H or C−O−C stretching of carbohydrate), 930 (vibration of glycosidic bond), and 851 cm^{-1} (deformation of C−H and CH_2) were observed in the pure starch (Pelissari, Andrade-Mahecha, do Amaral Sobral, & Menegalli, 2013).

Considering the WSM spectrum, an intramolecular hydroxyl stretching was observed at approximately 3285 cm^{-1} (Hong et al., 2016). The characteristic peaks at 2924 cm^{-1} (C−H bond stretching of CH_2–CH_3 group), 2060 cm^{-1} (stretching of N−C−S), 1604 cm^{-1} (C−O

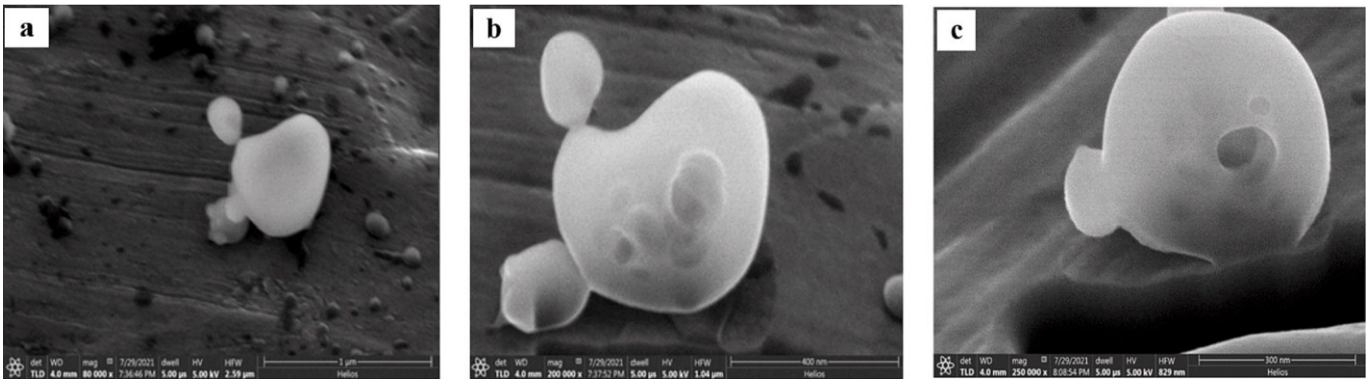

Fig. 4. FIB-SEM images of $SWTC_{30}$ nanocapsules: (a) surface structure, (b) internal structure, (c) nanocapsule with hollow pore. Abbreviations: SW, starch-water soluble yellow mustard mucilage; TC, thymol-carvacrol mixture; $SWTC_{30}$, SW with 30 % TC.

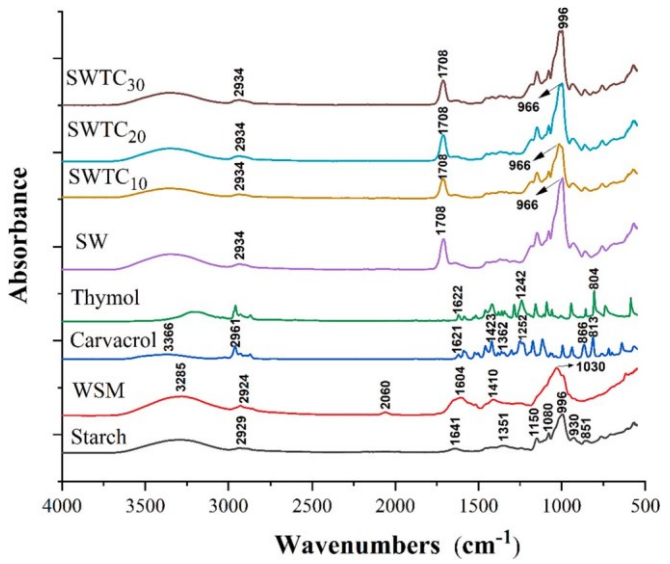

Fig. 5. FTIR spectra of pure starch, WSM, carvacrol, thymol, and nanocapsules (SW, $SWTC_{10}$, $SWTC_{20}$, and $SWTC_{30}$).

stretching of amide I), 1410 cm^{-1} (stretching of C−OH bond), and 1030 cm^{-1} (prominent carbohydrate peak due to C−OH or C−O−C stretching) were also seen (Hadad & Goli, 2018; Ubeyitogullari & Ciftci, 2020).

The carvacrol's signature IR bands were identified at 3366 cm^{-1} (intramolecular O−H stretching from the phenolic methyl group) and 2961 cm^{-1} (C−H stretching from the phenolic isopropyl group) (Keawchaoon & Yoksan, 2011). Furthermore, the spectrum displayed bands at 1423 and 1362 cm^{-1} (C−H bond deformation), 866 and 813 cm^{-1} (C−C stretching of phenol), and 1252 cm^{-1} (stretching of C−O). The peaks between 1621 and 1422 cm^{-1} correspond to the C−C stretching of benzene ring (Altan et al., 2018; Arrieta, Peltzer, del Carmen Garrigo´s, & Jim´enez, 2013).

The thymol displayed a similar spectrum to carvacrol as they are isomers. Thymol's signature bands were identified between 1242 and 1622 cm^{-1} (O−H bending, stretching of C−C, and C−O stretching of phenol) (Celebioglu, Yildiz, & Uyar, 2018). Thymol (804 cm^{-1}) and carvacrol (813 cm^{-1}) are generally distinguished using their intense band attributed to out-of-plane C−H vibrations (Schulz, O¨ zkan, Baranska, Krüger, & O¨ zcan, 2005).

The spectra of electrospray capsules were similar, which could be ascribed to a large amount of starch on the capsules' surface, thereby masking the effect of WSM, thymol, and carvacrol. Nordin, Othman, Rashid, and Basha (2020) reported similar observations in the starch film loaded with thymol and glycerol.

In our results, the capsules had a broad band between 3000 and 3700 cm^{-1}, which is most likely associated with the stretching vibration of hydroxyl groups belonging to starch, WSM, thymol, and carvacrol. The change in peak position denotes the interaction among the polysaccharides and/or bioactive compounds. It was noticed that the capsules displayed a small peak at 2934 cm^{-1} due to the C−H stretching vibration of starch and WSM. The actual peak related to C−H stretching was found in 2929 cm^{-1} (starch) and 2924 cm^{-1} (WSM), but in the fabricated capsules, it shifted to 2934 cm^{-1} showing the interaction between polysaccharides (Celebioglu, Kayaci-Senirmak, I˙pek, Durgun, & Uyar, 2016). The strong band that appeared at 1708 cm^{-1} (C−O group) is attributed to the COOH moiety of formic acid, the solvent used for electrospray (Fonseca et al., 2019). The band at 996 cm^{-1} displayed an increase in peak intensity, possibly due to the intermolecular hydrogen bonding between starch and WSM. No new peaks were noted with the TC incorporation, showing that the thymol and carvacrol were entrapped physically without chemical interactions with the polysaccharides.

3.6. Release kinetics of encapsulated TC

In the current study, the potential of WSM in modulating the release kinetics was explored by comparing the SW capsules with starch capsules both loaded with TC (30 % w/w). Fig. 6 shows the release behavior of TC from $SWTC_{30}$ and STC_{30} capsules.

The release pattern of bioactive compounds is essential to exhibit the ability to modulate the release kinetics according to the purpose of applying the capsules. The release kinetics could be adjusted by modifying the matrix performance. In the antimicrobial packaging system, if the releasing ability of the TC from the capsules is slow, bacteria could be developed in the food matrix before the TC is released. Instead, if the release is fast, the TC could diffuse into the food matrix and might not be adhering at the surface of the food for inhibiting bacterial growth (Altan et al., 2018).

As illustrated in Fig. 6, the TC gradually released from 0 to 120 h from the $SWTC_{30}$ capsules, displaying a controlled release behavior. At the end of the 7th h, approximately 40.6 % of encapsulated TC was released from the capsules due to low-intense burst release. The rest of the encapsulated content was released gradually up to 120 h. Keawchaoon et al. (2011) observed a similar result, showing burst release at 6th h followed by a gradual release of encapsulated carvacrol.

In $SWTC_{30}$ capsules, strong intermolecular forces existed among the hydroxyl groups of starch and WSM molecules. The intermolecular forces can maintain a matrix structure and delay the TC release. In addition, no surface porosity was observed in the SW polymer matrix (Fig. 3a), which may help prevent the entry of any dissolution medium to an extent. Further, WSM could have retained the TC molecules by hydrophobic bonding that holds the molecules against the diffusion force, thereby controlling the TC release.

Considering the starch capsules, a high-intensity burst release of TC (70.7 %) occurred at 7th h (Fig. 6). After that point, no significant release was observed from the capsules. This observation might be related to the weak structure among molecules. In addition, the starch capsules were irregular-shaped due to incomplete TC entrapment, leading to a high amount of surface TC content, thereby causing burst release of surface TC (Flamminii et al., 2020).

Encapsulated TC could undergo various mechanisms such as diffusion, surface erosion, desorption, and/or disintegration to get released from the nanocapsules (Rezaeinia, Emadzadeh, & Ghorani, 2020). To identify the specific mechanism through which the encapsulated TC was released from $SWTC_{30}$ capsules, different mathematical models, namely Ritger-Peppas, Peppas-Sahlin, Higuchi, Kopcha, and zero-order, were used (Costa & Lobo, 2001; Higuchi, 1963; Kopcha, Tojo, & Lordi, 1990; Peppas & Sahlin, 1989; Ritger & Peppas, 1987). The releasing pattern was fitted in the models, and the kinetics parameters were calculated (Table 2). Mathematical models that displayed the highest coefficient of determination (R^2) and adjusted R^2 were selected to describe the release mechanism of TC. Ritger-Peppas, Kopcha, and Higuchi models showed a good fit with an R^2 value of 0.991, 0.983, and 0.983 and adjusted R^2 values of 0.981, 0.974, and 0.968, respectively.

The diffusion exponent (n) in Ritger-Peppas was <0.45, indicating that the main mechanism involved in the release of TC from the spherical-shaped nanocapsules is Case-I transport, termed as "Fickian diffusion" (Ritger & Peppas, 1987).

Considering the Kopcha model, the A to B ratio was >1, concluding that the primary mechanism involved in the TC release is the Fickian diffusion (Kopcha et al., 1990). This observation might be attributed to the hydrophilic nature of starch and WSM, which allows gradual penetration of water molecules into their structure, causing the release of TC in a sustained manner (Fahami & Fathi, 2018).

Similar to Ritger-Peppas and Kopcha, the releasing profile fitted well with the Higuchi, pointing out the Fickian diffusion (Higuchi, 1963). In a study, the oregano oil was encapsulated in soy protein isolate and gum

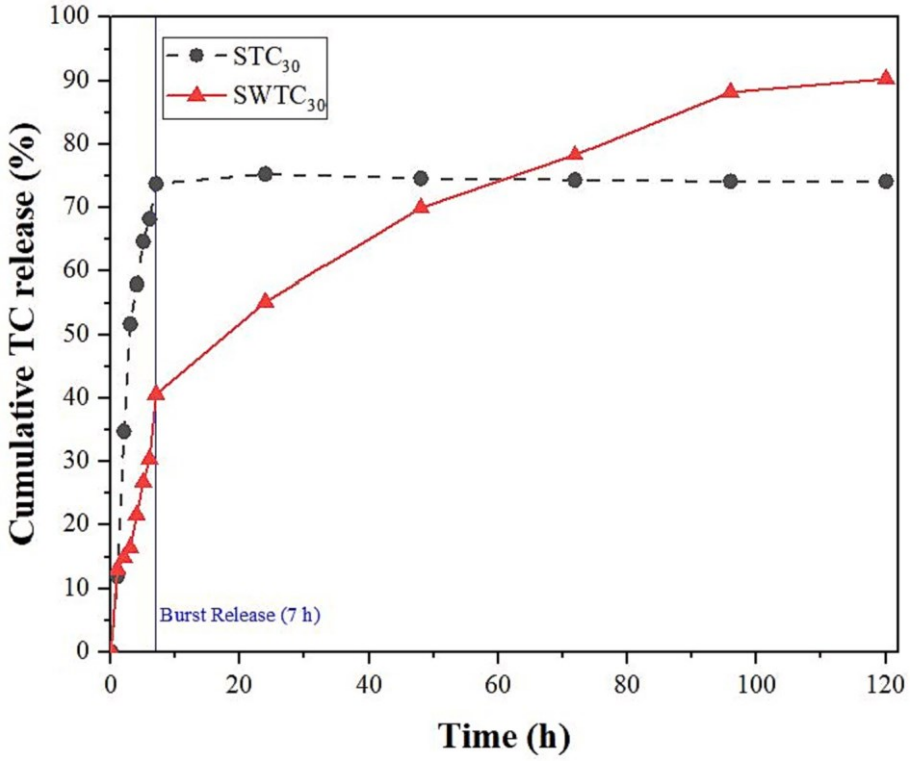

Fig. 6. Cumulative release (%) of TC from $SWTC_{30}$ and STC_{30} capsules. Abbreviations: SW, starch-water soluble yellow mustard mucilage; TC, thymol-carvacrol mixture; $SWTC_{30}$, SW with 30 % TC; STC_{30}, starch capsules with 30 % TC.

Table 2
Mathematical models for analyzing the release behavior of TC from $SWTC_{30}$ capsules. Abbreviations: M_t is the amount of TC (mg) released from the capsules at time t; M_0 is the initial amount of TC (mg) in the capsules

Kinetic model	Equation	Exponent and release mechanism	Results
Zero order	$M_t/M_0 = k \times t$	"k" is the release constant "t" is the time	R^2 = 0.925 R^2_{adj} = 0.907 k = 0.955
Ritger-Peppas	$M_t/M_0 = k \times t^n$	"k" is the release constant "t" is the time "n" is the release exponent $n \leq 0.45$ denotes "Fickian diffusion" $0.45 < n < 0.89$ denotes "non-Fickian" diffusion $0.89 < n < 1$ denotes "Erosion"	R^2 = 0.991 R^2_{adj} = 0.981 k = 14.83 n = 0.388
Higuchi	$M_t/M_0 = k \times t^{0.5}$	"k" is the release constant "t" is the time	R^2 = 0.983 R^2_{adj} = 0.968 k = 9.33
Kopcha	$M_t = A \times t^{1/2} + B \times t$	"A" denotes diffusion rate constant "B" denotes erosion rate constant "t" is the time A/B > 1 denotes "diffusion mechanism" A/B < 1 denotes "erosion mechanism"	R^2 = 0.983 R^2_{adj} = 0.974 A = 9.24 B = 0.01
Peppas-Sahlin	$M_t/M_0 = k_1t^m + k_2t^{2m}$	k_1 denotes diffusion rate constant k_2 denotes erosion rate constant "t" is the time $k_1/k_2 > 1$ denotes "Fickian diffusion mechanism" $k_1/k_2 < 1$ denotes "erosion mechanism" $k_1/k_2 = 1$ denotes "both erosion and diffusion mechanism"	R^2 = 0.822 R^2_{adj} = 0.804 k_1 = 0.545 k_2 = 0.06

acacia matrix (Xue, Gu, Wang, Li, & Adhikari, 2019). Similar to our results, the bioactive compounds were released in a controlled manner but up to 330 h. The authors' fitted the data in the Peppas model and concluded that the gradual release was mainly due to the diffusion mechanism. Other researchers have also observed Fickian diffusion as the prominent mechanism in releasing bioactive compounds (e.g., polyphenols, essential oils, etc.) (Go´mez-Mascaraque, Lagaro´n, & Lo´pez-Rubio, 2015; Rezaeinia et al., 2019; Rezaeinia et al., 2020). In our study, it could be concluded that the encapsulated $SWTC_{30}$ capsules were stable and released TC gradually by the Fickian diffusion mechanism.

4. Conclusion

This study encapsulated highly volatile TC within the SW matrix without using toxic solvents or high temperatures by electrospray. Optimization of processing parameters and solution dynamics assisted in generating uniform nanocapsules with an average diameter ranging from 73.09 to 94.46 nm. A higher EE of 84.10 % was achieved in $SWTC_{30}$ capsules. The morphological study using SEM confirmed the non-porous spherical structure of nanocapsules. The internal structure analyzed by FIB-SEM displayed the multicore structures within the wall layer. FTIR spectra indicated no molecular interaction between SW matrix and TC in the capsules, showing that the TC was entrapped physically without undergoing chemical interactions. However, there were intermolecular interactions between WSM and starch, confirmed by the peak at 2934 and 996 cm^{-1}. These interactions helped to entrap the TC physically by forming a compact structure surrounding the multicore layer. Release kinetics of TC from $SWTC_{30}$ capsules followed a controlled release pattern up to 120 h. The releasing pattern fits well with the Ritger-Peppas, Kopcha, and Higuchi model, indicating that the Fickian diffusion mechanism was prominent for TC release. Overall results showed that the electrospray SW matrix could act as a delivery carrier for encapsulating hydrophobic bioactive compounds. Furthermore, $SWTC_{30}$ capsules are recommended explicitly for antimicrobial

packaging. Future investigation over real food is ongoing to evaluate its shelf-life extension ability and impact on the organoleptic property of fresh foods.

CRediT authorship contribution statement

Anto Pradeep Raja Charles: Investigation, Conceptualization, Data curation, Writing-original draft, Writing-review & editing.

Richard Mu: Supervision, Writing-review & editing, Validation, Methodology.

Tony Z. Jin: Supervision, Writing-review & editing, Methodology.

Deyu Li: Writing-review & editing, Methodology.

Zhiliang Pan: Data curation.

Sudipta Rakshit: Data curation, Writing-review & editing.

Steve W. Cui: Writing-review & editing.

Ying Wu: Conceptualization, Writing-review & editing, Supervision, Project administration, Resources, Funding.

Declaration of competing interest

The authors declare that they have no known competing financial interests or personal relationships that could have appeared to influence the work reported in this paper.

Data availability

Data will be made available on request.

Acknowledgment

This research is financially aided by the USDA National Institute of Food and Agriculture (USDA NIFA), Evans-Allen Project, Grant Number [1025030].

References

Altan, A., Aytac, Z., & Uyar, T. (2018). Carvacrol loaded electrospun fibrous films from zein and poly (lactic acid) for active food packaging. *Food Hydrocolloids, 81*, 48–59. https://doi.org/10.1016/j.foodhyd.2018.02.028

Arrieta, M. P., Peltzer, M. A., del Carmen Garrigo´s, M., & Jim´enez, A. (2013). Structure and mechanical properties of sodium and calcium caseinate edible active films with carvacrol. *Journal of Food Engineering, 114*(4), 486–494. https://doi.org/10.1016/j.jfoodeng.2012.09.002

Atay, E., Fabra, M. J., Martínez-Sanz, M., Gomez-Mascaraque, L. G., Altan, A., & Lopez-Rubio, A. (2018). Development and characterization of chitosan/gelatin electrosprayed microparticles as food grade delivery vehicles for anthocyanin extracts. *Food Hydrocolloids, 77*, 699–710. https://doi.org/10.1016/j.foodhyd.2017.11.011

Atta, O. M., Manan, S., Shahzad, A., Ul-Islam, M., Ullah, M. W., & Yang, G. (2022). Biobased materials for active food packaging: A review. *Food Hydrocolloids, 125*, Article 107419. https://doi.org/10.1016/j.foodhyd.2021.107419

Capron, I., Robert, P., Colonna, P., Brogly, M., & Planchot, V. (2007). Starch in rubbery and glassy states by FTIR spectroscopy. *Carbohydrate Polymers, 68*(2), 249–259. https://doi.org/10.1016/j.carbpol.2006.12.015

Celebioglu, A., Kayaci-Senirmak, F., I˙pek, S., Durgun, E., & Uyar, T. (2016). Polymer-free nanofibers from vanillin/cyclodextrin inclusion complexes: High thermal stability, enhanced solubility and antioxidant property. *Food & Function, 7*(7), 3141–3153. https://doi.org/10.1039/C6FO00569A

Celebioglu, A., Yildiz, Z. I., & Uyar, T. (2018). Thymol/cyclodextrin inclusion complex nanofibrous webs: Enhanced water solubility, high thermal stability and antioxidant property of thymol. *Food Research International, 106*, 280–290. https://doi.org/10.1016/j.foodres.2017.12.062

Charles, A. P. R., Jin, T. Z., Mu, R., & Wu, Y. (2021). Electrohydrodynamic processing of natural polymers for active food packaging: A comprehensive review. *Comprehensive Reviews in Food Science and Food Safety, 20*(6), 6027–6056. https://doi.org/10.1111/1541-4337.12827

Cheng, J., Wang, H., Kang, S., Xia, L., Jiang, S., Chen, M., & Jiang, S. (2019). An active packaging film based on yam starch with eugenol and its application for pork preservation. *Food Hydrocolloids, 96*, 546–554. https://doi.org/10.1016/j.foodhyd.2019.06.007

Costa, P., & Lobo, J. M. S. (2001). Modeling and comparison of dissolution profiles. *European Journal of Pharmaceutical Sciences, 13*(2), 123–133. https://doi.org/10.1016/S0928-0987(01)00095-1

Cui, L., Kimmel, J., Zhou, L., Rao, J., & Chen, B. (2020). Combining solid dispersion-based spray drying with cyclodextrin to improve the functionality and mitigate the beany odor of pea protein isolate. *Carbohydrate Polymers, 245*, Article 116546. https://doi.org/10.1016/j.carbpol.2020.116546

Cui, S. W., Eskin, M. A., Wu, Y., & Ding, S. (2006). Synergisms between yellow mustard mucilage and galactomannans and applications in food products—A mini review. *Advances in Colloid and Interface Science, 128*, 249–256. https://doi.org/10.1016/j.cis.2006.11.012

de Souza, E. J. D., Kringel, D. H., Dias, A. R. G., & da Rosa Zavareze, E. (2021). Polysaccharides as wall material for the encapsulation of essential oils by electrospun technique. *Carbohydrate Polymers, 265*, Article 118068. https://doi.org/10.1016/j.carbpol.2021.118068

Fahami, A., & Fathi, M. (2018). Development of cress seed mucilage/PVA nanofibers as a novel carrier for vitamin a delivery. *Food Hydrocolloids, 81*, 31–38. https://doi.org/10.1016/j.foodhyd.2018.02.008

Fani, N., Enayati, M. H., Rostamabadi, H., & Falsafi, S. R. (2022). Encapsulation of bioactives within electrosprayed κ-carrageenan nanoparticles. *Carbohydrate Polymers, 294*, Article 119761. https://doi.org/10.1016/j.carbpol.2022.119761

Flamminii, F., Di Mattia, C. D., Nardella, M., Chiarini, M., Valbonetti, L., Neri, L., & Pittia, P. (2020). Structuring alginate beads with different biopolymers for the development of functional ingredients loaded with olive leaves phenolic extract. *Food Hydrocolloids, 108*, Article 105849. https://doi.org/10.1016/j.foodhyd.2020.105849

Fonseca, L. M., dos Santos Cruxen, C. E., Bruni, G. P., Fiorentini, Aˆ. M., da Rosa Zavareze, E., Lim, L. T., & Dias, A. R. G. (2019). Development of antimicrobial and antioxidant electrospun soluble potato starch nanofibers loaded with carvacrol. *International Journal of Biological Macromolecules, 139*, 1182–1190. https://doi.org/10.1016/j.ijbiomac.2019.08.096

Ghorani, B., & Tucker, N. (2015). Fundamentals of electrospinning as a novel delivery vehicle for bioactive compounds in food nanotechnology. *Food Hydrocolloids, 51*, 227–240. https://doi.org/10.1016/j.foodhyd.2015.05.024

Go´mez-Mascaraque, L. G., Lagaro´n, J. M., & Lo´pez-Rubio, A. (2015). Electrosprayed gelatin submicroparticles as edible carriers for the encapsulation of polyphenols of interest in functional foods. *Food Hydrocolloids, 49*, 42–52. https://doi.org/10.1016/j.foodhyd.2015.03.006

Hadad, S., & Goli, S. A. H. (2018). Fabrication and characterization of electrospun nanofibers using flaxseed (Linum usitatissimum) mucilage. *International Journal of Biological Macromolecules, 114*, 408–414. https://doi.org/10.1016/j.ijbiomac.2018.03.154

Hajimehdipoor, H., Shekarchi, M., Khanavi, M., Adib, N., & Amri, M. (2010). A validated high performance liquid chromatography method for the analysis of thymol and carvacrol in Thymus vulgaris L. volatile oil. *Pharmacognosy Magazine, 6*(23), 154. https://doi.org/10.4103/2F0973-1296.66927

Hamaker, B. R. (2021). Current and future challenges in starch research. *Current Opinion in Food Science, 40*, 46–50. https://doi.org/10.1016/j.cofs.2021.01.003

Higuchi, T. (1963). Mechanism of sustained-action medication. Theoretical analysis of rate of release of solid drugs dispersed in solid matrices. *Journal of Pharmaceutical Sciences, 52*(12), 1145–1149. https://doi.org/10.1002/jps.2600521210

Hong, J., Chen, R., Zeng, X. A., & Han, Z. (2016). Effect of pulsed electric fields assisted acetylation on morphological, structural and functional characteristics of potato starch. *Food Chemistry, 192*, 15–24. https://doi.org/10.1016/j.foodchem.2015.06.058

Human, C., De Beer, D., Van Der Rijst, M., Aucamp, M., & Joubert, E. (2019). Electrospraying as a suitable method for nanoencapsulation of the hydrophilic bioactive dihydrochalcone, aspalathin. *Food Chemistry, 276*, 467–474. https://doi.org/10.1016/j.foodchem.2018.10.016

Jain, A., Dasgupta, N., Ranjan, S., Singh, V., Singh, H., Purohit, S. D.Samanta, S. K., ... (2021). Whey protein based electrosprayed nanospheres for encapsulation and controlled release of bioactive compounds from Tinospora cordifolia extract. *Innovative Food Science & Emerging Technologies, 69*, Article 102671. https://doi.org/10.1016/j.ifset.2021.102671

Keawchaoon, L., & Yoksan, R. (2011). Preparation, characterization and in vitro release study of carvacrol-loaded chitosan nanoparticles. *Colloids and Surfaces B: Biointerfaces, 84*(1), 163–171. https://doi.org/10.1016/j.colsurfb.2010.12.031

Kopcha, M., Tojo, K. J., & Lordi, N. G. (1990). Evaluation of methodology for assessing release characteristics of thermosoftening vehicles. *Journal of Pharmacy and Pharmacology, 42*(11), 745–751. https://doi.org/10.1111/j.2042-7158.1990.tb07014.x

Kuai, L., Liu, F., Chiou, B. S., Avena-Bustillos, R. J., McHugh, T. H., & Zhong, F. (2021). Controlled release of antioxidants from active food packaging: A review. *Food Hydrocolloids, 120*, Article 106992. https://doi.org/10.1016/j.foodhyd.2021.106992

Li, K. K., Yin, S. W., Yin, Y. C., Tang, C. H., Yang, X. Q., & Wen, S. H. (2013). Preparation of water-soluble antimicrobial zein nanoparticles by a modified antisolvent approach and their characterization. *Journal of Food Engineering, 119*(2), 343–352. https://doi.org/10.1016/j.jfoodeng.2013.05.038

Limbo, S., & Khaneghah, A. M. (2015). Active packaging of foods and its combination with electron beam processing. In S. Pillai, & S. Shayanfar (Eds.), *Electron beam pasteurization and complementary food processing technologies* (pp. 195–217). Woodhead Publishing.

Liu, H., Eskin, N. M., & Cui, S. W. (2003). Interaction of wheat and rice starches with yellow mustard mucilage. *Food Hydrocolloids, 17*(6), 863–869. https://doi.org/10.1016/S0268-005X(03)00107-3

Liu, H., Eskin, N. M., & Cui, S. W. (2006). Effects of yellow mustard mucilage on functional and rheological properties of buckwheat and pea starches. *Food Chemistry, 95*(1), 83–93. https://doi.org/10.1016/j.foodchem.2004.12.027

Liu, Y., Li, S., Li, H., Hossen, M. A., Sameen, D. E., Dai, J.Lee, K., ... (2021). Synthesis and properties of core-shell thymol-loaded zein/shellac nanoparticles by coaxial

electrospray as edible coatings. *Materials & Design, 212*, Article 110214. https://doi.org/10.1016/j.matdes.2021.110214

Marchese, A., Orhan, I. E., Daglia, M., Barbieri, R., Di Lorenzo, A., Nabavi, S. F., & Nabavi, S. M. (2016). Antibacterial and antifungal activities of thymol: A brief review of the literature. *Food Chemistry, 210*, 402–414. https://doi.org/10.1016/j.foodchem.2016.04.111

McClements, D. J. (2015). *Food emulsions: Principles, practices, and techniques*. CRC Press.

Niu, B., Shao, P., & Sun, P. (2020). Ultrasound-assisted emulsion electrosprayed particles for the stabilization of β-carotene and its nutritional supplement potential. *Food Hydrocolloids, 102*, Article 105634. https://doi.org/10.1016/j.foodhyd.2019.105634

Niu, B., Shao, P., Luo, Y., & Sun, P. (2020). Recent advances of electrosprayed particles as encapsulation systems of bioactives for food application. *Food Hydrocolloids, 99*, Article 105376. https://doi.org/10.1016/j.foodhyd.2019.105376

Nordin, N., Othman, S. H., Rashid, S. A., & Basha, R. K. (2020). Effects of glycerol and thymol on physical, mechanical, and thermal properties of corn starch films. *Food Hydrocolloids, 106*, Article 105884. https://doi.org/10.1016/j.foodhyd.2020.105884

Park, C. H., & Lee, J. (2009). Electrosprayed polymer particles: Effect of the solvent properties. *Journal of Applied Polymer Science, 114*(1), 430–437. https://doi.org/10.1002/app.30498

Paximada, P., Echegoyen, Y., Koutinas, A. A., Mandala, I. G., & Lagaron, J. M. (2017). Encapsulation of hydrophilic and lipophilized catechin into nanoparticles through emulsion electrospraying. *Food Hydrocolloids, 64*, 123–132. https://doi.org/10.1016/j.foodhyd.2016.11.003

Pelissari, F. M., Andrade-Mahecha, M. M., do Amaral Sobral, P. J., & Menegalli, F. C. (2013). Comparative study on the properties of flour and starch films of plantain bananas (Musa paradisiaca). *Food Hydrocolloids, 30*(2), 681–690. https://doi.org/10.1016/j.foodhyd.2012.08.007

Peppas, N. A., & Sahlin, J. J. (1989). A simple equation for the description of solute release. III. Coupling of diffusion and relaxation. *International Journal of Pharmaceutics, 57*(2), 169–172. https://doi.org/10.1016/0378-5173(89)90306-2

P´erez-Co´rdoba, L. J., Norton, I. T., Batchelor, H. K., Gkatzionis, K., Spyropoulos, F., & Sobral, P. J. (2018). Physico-chemical, antimicrobial and antioxidant properties of gelatin-chitosan based films loaded with nanoemulsions encapsulating active compounds. *Food Hydrocolloids, 79*, 544–559. https://doi.org/10.1016/j.foodhyd.2017.12.012

P´erez-Masia´, R., Lo´pez-Nicol´as, R., Periago, M. J., Ros, G., Lagaron, J. M., & Lo´pez-Rubio, A. (2015). Encapsulation of folic acid in food hydrocolloids through nanospray drying and electrospraying for nutraceutical applications. *Food Chemistry, 168*, 124–133. https://doi.org/10.1016/j.foodchem.2014.07.051

Rehman, A., Ahmad, T., Aadil, R. M., Spotti, M. J., Bakry, A. M., Khan, I. M.Tong, Q., ... (2019). Pectin polymers as wall materials for the nano-encapsulation of bioactive compounds. *Trends in Food Science & Technology, 90*, 35–46. https://doi.org/10.1016/j.tifs.2019.05.015

Rezaeinia, H., Emadzadeh, B., & Ghorani, B. (2020). Electrospun balangu (Lallemantia royleana) hydrocolloid nanofiber mat as a fast-dissolving carrier for bergamot essential oil. *Food Hydrocolloids, 100*, Article 105312. https://doi.org/10.1016/j.foodhyd.2019.105312

Rezaeinia, H., Ghorani, B., Emadzadeh, B., & Tucker, N. (2019). Electrohydrodynamic atomization of Balangu (Lallemantia royleana) seed gum for the fast-release of Mentha longifolia L. essential oil: Characterization of nanocapsules and modeling the kinetics of release. *Food Hydrocolloids, 93*, 374–385. https://doi.org/10.1016/j.foodhyd.2019.02.018

Ritger, P. L., & Peppas, N. A. (1987). A simple equation for description of solute release I. Fickian and non-fickian release from non-swellable devices in the form of slabs, spheres, cylinders or discs. *Journal of Controlled Release, 5*(1), 23–36. https://doi.org/10.1016/0168-3659(87)90035-6

Schulz, H., O¨zkan, G., Baranska, M., Krüger, H., & O¨zcan, M. (2005). Characterisation of essential oil plants from Turkey by IR and Raman spectroscopy. *Vibrational Spectroscopy, 39*(2), 249–256. https://doi.org/10.1016/j.vibspec.2005.04.009

Shakeri, M., Razavi, S. H., & Shakeri, S. (2019). Carvacrol and astaxanthin co-entrapment in beeswax solid lipid nanoparticles as an efficient nano-system with dual antioxidant and anti-biofilm activities. *LWT- Food Science and Technology, 107*, 280–290. https://doi.org/10.1016/j.lwt.2019.03.031

Soleimanifar, M., Jafari, S. M., & Assadpour, E. (2020). Encapsulation of olive leaf phenolics within electrosprayed whey protein nanoparticles; production and characterization. *Food Hydrocolloids, 101*, Article 105572. https://doi.org/10.1016/j.foodhyd.2019.105572

Sun, C., & Gunasekaran, S. (2009). Effects of protein concentration and oil-phase volume fraction on the stability and rheology of menhaden oil-in-water emulsions stabilized by whey protein isolate with xanthan gum. *Food Hydrocolloids, 23*(1), 165–174. https://doi.org/10.1016/j.foodhyd.2007.12.006

Sun, X., Cameron, R. G., & Bai, J. (2020). Effect of spray-drying temperature on physicochemical, antioxidant and antimicrobial properties of pectin/sodium alginate microencapsulated carvacrol. *Food Hydrocolloids, 100*, Article 105420. https://doi.org/10.1016/j.foodhyd.2019.105420

Ubeyitogullari, A., & Ciftci, O. N. (2020). Fabrication of bioaerogels from camelina seed mucilage for food applications. *Food Hydrocolloids, 102*, Article 105597. https://doi.org/10.1016/j.foodhyd.2019.105597

Wu, Y., Cui, W., Eskin, N. A. M., Goff, H. D., & Nikiforuk, J. (2011). NMR analysis of a methylated non-pectic polysaccharide from water soluble yellow mustard mucilage. *Carbohydrate Polymers, 84*(1), 69–75. https://doi.org/10.1016/j.carbpol.2010.10.058

Wu, Y., Eskin, N. A. M., Cui, W., & Pokharel, B. (2015). Emulsifying properties of water soluble yellow mustard mucilage: A comparative study with gum arabic and citrus pectin. *Food Hydrocolloids, 47*, 191–196. https://doi.org/10.1016/j.foodhyd.2015.01.020

Wu, Y., Hui, D., Eskin, N. A. M., & Cui, S. W. (2016). Water-soluble yellow mustard mucilage: A novel ingredient with potent antioxidant properties. *International Journal of Biological Macromolecules, 91*, 710–715. https://doi.org/10.1016/j.ijbiomac.2016.05.088

Xue, F., Gu, Y., Wang, Y., Li, C., & Adhikari, B. (2019). Encapsulation of essential oil in emulsion based edible films prepared by soy protein isolate-gum acacia conjugates. *Food Hydrocolloids, 96*, 178–189. https://doi.org/10.1016/j.foodhyd.2019.05.014

Yilmaz, M. T., Yilmaz, A., Akman, P. K., Bozkurt, F., Dertli, E., Basahel, A., & Sagdic, O. (2019). Electrospraying method for fabrication of essential oil loaded-chitosan nanoparticle delivery systems characterized by molecular, thermal, morphological and antifungal properties. *Innovative Food Science & Emerging Technologies, 52*, 166–178. https://doi.org/10.1016/j.ifset.2018.12.005

Zhang, W., Jiang, H., Rhim, J. W., Cao, J., & Jiang, W. (2022). Effective strategies of sustained release and retention enhancement of essential oils in active food packaging films/coatings. *Food Chemistry, 367*, Article 130671. https://doi.org/10.1016/j.foodchem.2021.130671